The role of solvent additive in metal nano-composite doped thin film organic solar cell

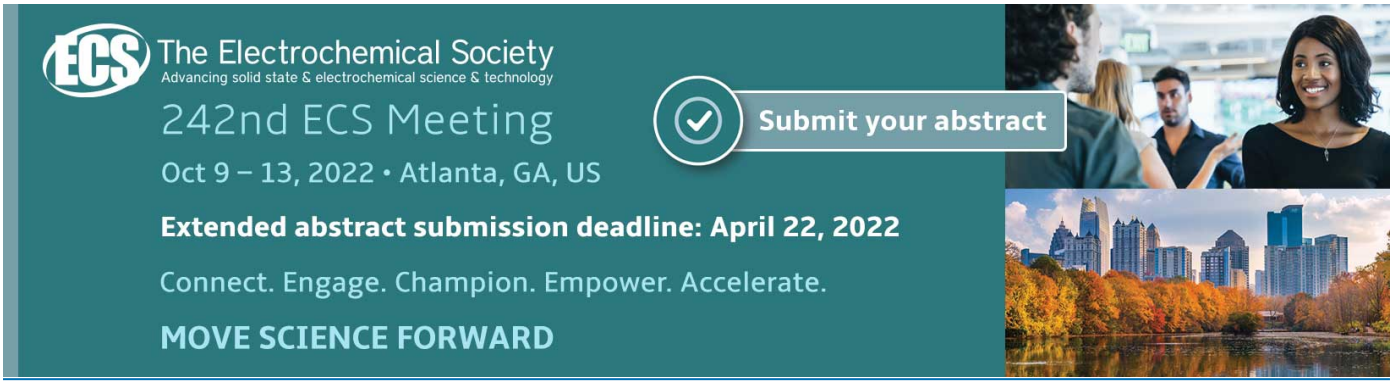

The role of solvent additive in metal nano-composite doped thin film organic solar cell

[1]Kesinro, R. O., [2]Boyo, A. O, [1]Akinyemi, M. L., [3]Hamed, M.S.G., [4]Kaviyarasu K., [3]Mola, G. T., [1,5]Emetere, M. E., [1]Aizebeokhai, A. P.
[1]Covenant University, Ota, Ogun State, Nigeria.,
[2]Lagos State University, Ojo, Lagos State.,
[3]University of Kwazulu-Natal, School of Chemistry & Physics, Pietermaritzburg, South Africa
[4]Nanosciences African network, Materials Research Group, iThemba LABS- National Research Foundation, 1 Old Faure Road, 7129, PO Box 722, Somerset West, Western Cape Province, South Africa
[5]Department of Mechanical Engineering Science, University of Johannesburg, South Africa.

Corresponding author: olakesinro02@gmail.com

Abstract In this study, organic solar cells (OSCs) were designed using the solution processing method based on spin coating. The influence of solvent additive (1-chloronapthalene (CN)) and cadmium doped barium nitrate nanoparticle incorporated into the photoactive medium based on poly(3-hexylthiophene-2,5-diyl (P3HT): [6,6]-phenyl-C61-butyric acid methyl ester (PCBM) was investigated. The power conversion efficiency of the pristine device was compared to the power conversion efficiency of the devices fabricated with 30v% of 1- chloronapthalene and different weight concentrations of nanoparticles. An optimum efficiency of 3.55 % was attained at 0.3 wt.% with solvent additive compared to 3.25 % obtained for the pristine device. This increase is attributed to a rise in charge transport of 5.32×10^{-2} $cm^2V^{-1}s^{-1}$. Further investigation on the morphological properties of the nanoparticles reveals the crystalline nature of the nanoparticle.

Keywords: Nanoparticle; power conversion efficiency; solvent additive

1. Introduction

Efficiencies of solar cells is an extreme controlling factor (Abodunrin *et al.*, 2018). New photovoltaic devices built on less expensive organic semiconductor materials have been fabricated for use to convert solar energy to electricity. These organic semiconductor materials utilized in fabricating OSCs hold the advantage of low cost of production. This has led to enormous acknowledgement and intense research interest in the design of OSCs as a substitute to silicon based solar cells (Huang, *et al.,* 2017; Kong, Wang, Liu & Yu, 2017; Xing, Wang, Kong, Yu & Jiang, 2017). Similarly, the lightweight and flexibility of OSC devices along with less unpleasant environmental effect are advantageous since they can be processed at high quantity when compared to other solar converters. (Ono, Leyden, Wang & Qi, 2016; Wang *et al.,* 2016). In an OSC, a mixture of donor and acceptor polymers, blended together results into a bulk heterojunction (BHJ), which is a very effective photoactive medium for absorption of light and carrier mobility (Yin *et al.,* 2017).

The overall efficiency of organic solar cell devices has constantly shown increase, with recent efficiencies up to ~15.6 % has been attained in the laboratory and improved OSC systems with non-fullerene acceptor materials have attained ~ 12 % efficiency. Although, extra attempts are presently researched upon to advance semiconducting polymer materials (Vyprachticky,

Demirtas, Dzhabarov & Cimrova, 2017; Chen & Zhang, 2017; Tong *et al.,* 2015). A steady increase with respect to efficiency of ~15.6 % has been reported and recorded, with laboratory efficiency reaching 10 % in 2012; and recently ~ above 16 % in optimized OSC with non-fullerene acceptor materials (Chen & Zhang, 2017; Tong *et al.,* 2015).

Crystalline silicon solar cells are estimated to have high efficiencies relative to organic solar cells. The low mobility of carriers in polymer has hindered the absorber medium thickness (≤ 100 nm) resulting in limited optical absorption (Green, Emery, Hishikawa, Warta & Dunlop, 2016; Choy & Ren, 2016). Therefore, improving the absorbance of the organic semiconductor remains a hinderance (Lim et al., 2016). Again, Fleetham *et al.* (2015) reiterated to boost both electrical and optical functions of OSCs in order to overcome the hurdles of increasing the power conversion efficiency, metal and non-metal nanoparticles are utilized. Also, these nanoparticles are used to improve light trapping in OSCs, since local surface plasmon resonance and scattering of incident light is induced by the nanoparticles in the absorber medium, thus improving the average path length for the light in the device (Zhou, Puente, Wang, Polavarapu, Santos, & Xu, 2016). Also, according to several researchers such as Kaviyarasu *et al.* (2019), high concentrations of NPs in the absorber layer decreases the current and FF magnitude of the cells as a consequence of the increased series resistance produced by high concentration of Zn-SWCNT in the medium. Similarly, the Jsc hinges strongly on the gap energy and FF depend on the film morphology leading to improved carrier mobility and photocurrent. Also, Song *et al.* (2017) asserted that using DIO additive increased the accumulation of PCBM in the photoactive medium, ensuing in higher FF and Jsc. Variations in Voc shown in Table 4.3 in the presence of the additive is as a result of low recombination od carriers following the improvement in film morphology as asserted by Perez *et al.* (2009).

The overall efficiency of BHJ-OSC devices is mostly established by the morphology of the photoactive medium (Jackson, Savoie, Marks, Chen & Ratner, 2015). There have been a number of approaches to enrich the morphology of the photoactive medium for instance the addition of solvent additives. The additive method has shown to be widely utilized for BHJ-OSCs with (Tran, Kim, Park & Cho, 2018). They tend to change the solubility of one or both, components, or the mutual miscibility between the donor and acceptor. Octanedithiol (ODT), diiodooctane (DIO), diphenyl ether (DPE) and chloronaphthalene (CN) are typical processing additives for BHJ-OSCs. Foertig *et al.* (2014) examined the effect of introducing DIO additive in the photoactive medium composed of PTB7 and $PC_{71}BM$. It results obtained indicate an improvement in device performance by weakening of the bimolecular recombination, due to significant morphology changes in the photoactive layer. Choi *et al.* (2015) used DPE to enhance the morphology of DT-PDPP2T-TT: $PC_{71}BM$ in films with a thickness of up to 300 nm, thereby improving device PCE from 3.2% to a remarkable 9.5%. In the same vein, Araujo *et al.* (2019) researched the impact of DIO additive on performance of BHJ-OSC using PTB7-Th: $PC_{71}BM$ blend as the photoactive medium. Pure chlorobenzene as a solvent or mixed with DIO were used in fabrication of the devices. It was evident that the consequence of DIO in the photoactive layer improved its morphology, leading to improvement in the photogenerated current and reduction in the recombination effect. Consequently, the enhancement in photocurrent is attributed to the breaking up of the $PC_{71}BM$ clusters (Oseni *et al,* 2019; Arbab *et al* 2019). This increment in the photocurrent is likely due to the disintegration of the $PC_{71}BM$ clusters and their better penetration in the polymer medium of PTB7-Th, which assists the separation of carrier-transfer states at the interfaces.

In this study we investigate the influence of solvent additive and nanoparticles on the working of bulk heterojunction organic solar cells based on P3HT: PCBM photoactive layer. Different experimental methods were utilized to characterize structural and surface properties of

nanoparticles which include XRD, AFM (atomic force microscopy), TEM (transmission electron microscopy), (Afolalu, Soetan, Ongbali, Abioye, & Oni, 2019).

2. Methodology

The fabrication of BHJ-OSC was achieved using the spin coating and vacuum deposition method. The PEDOT: PSS was coated on clean etched ITO for 60 s at 3500 rpm and further annealed in an oven for 20 min at 100 °C under laboratory conditions (Oseni & Mola, 2017). The absorber medium was prepared using a combination of P3HT and PCBM at a weight ratio of 1: 1 in 20 g/ml of chloroform solvent. In the same vein, cadmium doped barium nitrate (Cd doped (Ba $(NO_3)_2$) nanoparticles and chloronapthalene (CN) were introduced at different loading percentages ranging from (0.1 - 0.5 %) by using weight plus 30 v% chloronapthalene into the P3HT: PCBM mixture discussed above. At a regular temperature of 45 °C for 4 h the solutions were stirred on a hot plate to form an improved mix of the different molecules in the mixture. Deposition of the absorber medium on the PEDOT: PSS was done at 1200 rpm for 40 s by spin coating, then moved to the oven and annealed for 10 min at 90 °C. Lastly, at vacuum pressure of 1.00×10^{-7} mbar, a layer of LiF (0.4 nm) representing the electron transport layer and Al (60 nm) as the top electrode was deposited using the vacuum deposition machine (Oseni & Mola, 2017). Figure 1 was showing a schematic diagram of the fabricated device.

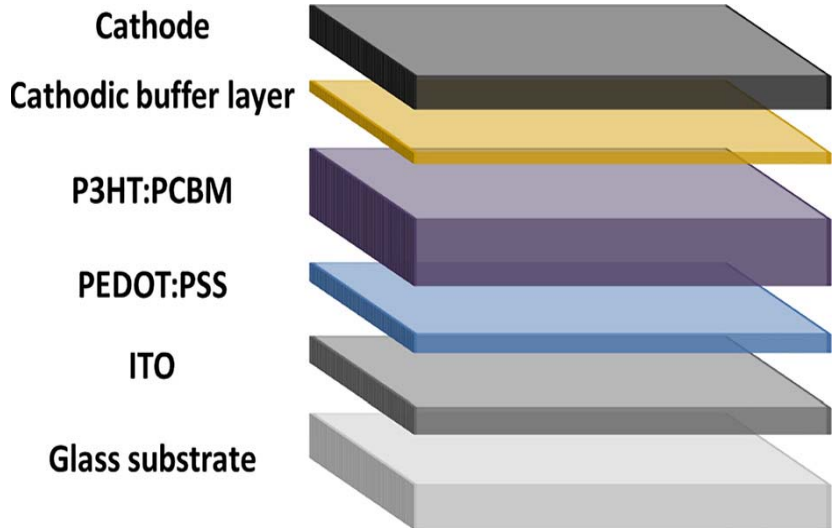

Figure 1: Schematic diagram of fabricated device
Source: Berger & Kim (2018).

3. Results and Discussion

The optical absorbance spectra of the devices incorporated with NPs and solvent additive was investigated. Figure 4.4 shows some identical absorption spectra for all the devices; two prominent peaks are observed between 350 - 400 nm and 500 - 550 nm with a hump around 600 nm. Furthermore, the absorption spectra of the devices are observed to be enhanced related to the undoped device. This is probable linked to mutual compensation of the P3HT and PCBM in addition to improved phase-separated

morphology of the absorber medium due to the introduction of the solvent additive. Also, enhancement in the absorption spectra could be attached to the altered π-π* bond in the photoactive layer. Ergete *et al.* (2015) asserted that in the presence of solvent additives there is generally a red shift to longer wavelengths in absorbance as observed in Figure 2. Also, this long shift in wavelength is explained to be as a consequence of the disbanding of PCBM cluster which separate and redistribute in the polymer chain enhancing the crystalline order. Similarly, Oseni & Mola (2019) studied the absorption pattern of the devices based PTB7: PCBM absorber layer doped with NPs and solvent additive. The results obtained showed pronounced absorption peaks and a red shift of almost 35 nm for the doped device similar to Figure 4.4. this change is said to be caused by the additive rather than NPs. The presence of fullerene molecules in the absorber layer is attributed to the vibronic shoulder observed. According to Seo *et al.* (2011) introducing additives into the absorber layer improves the solubility of the PCBM by increasing the alkyl chain length thereby causing a red shift in absorption. Introducing solvent additive primarily improves the absorption strength of devices observed in Figure 4.4. Meanwhile, Liu *et al.* (2001) implied that the physical interactions between the polymer chains could be influenced by the additives chain length thereby improving the absorption, morphology and efficiency of the device.

The photovoltaic parameters obtained for devices fabricated with various concentrations of NPs with solvent additive (1-chloronapthalene (CN)) (30%v.) are presented in Table 1. Figure 3 indicates the current density – voltage graphs under AM 1.5 conditions of P3HT: PCBM, NP, and CN active medium. An optimum PCE of 3.55 % for the BHJ-OSC fabricated with 0.3 wt.% NPs and solvent additive (CN) is obtained, exhibiting a V_{oc} of 0.46 V, J_{sc} of 17.05 mA/cm^2, FF of 45.03. Also, the least performing device is attained at 0.5 wt. % with V_{oc} of 0.49 V, J_{sc} of 10.31 mA/cm^2, FF of 41.13 and PCE of 2.11 %. An enhancement in FF is observed for the devices in Table 1. Also, an upgrading in the FF is probably as a result of improved morphology of the active medium due to the addition of CN. It is known that the addition of solvent additives helps in promoting phase separation of the polymer blends and creates nanoscale pure phase domains of interconnecting D/A interface which reduces trap assisted geminate recombination leading to an improved FF. It was observed that the devices embedded with NP and NPs (CN) showed an upgrade in J_{sc} and FF when compared to the pristine device. The NPs (CN) devices show an improved FF and a decrease in V_{oc} to pristine and NP only doped devices.

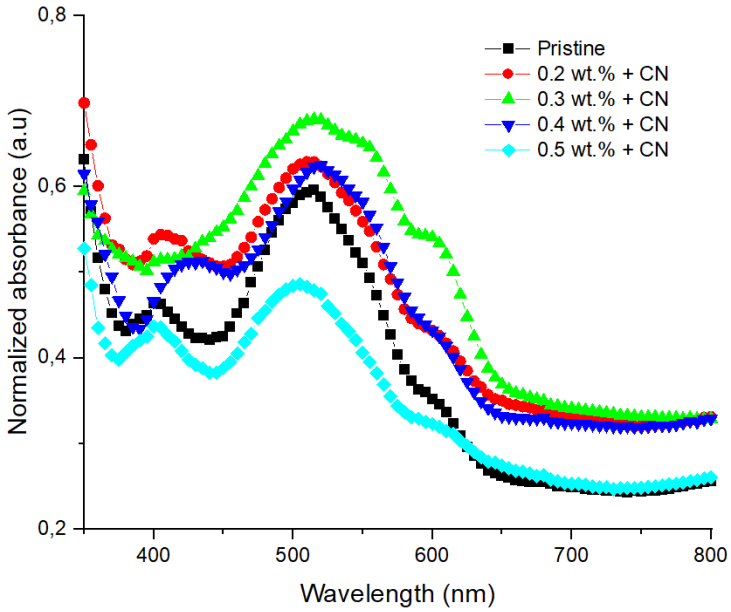

Figure 2: Optical absorption spectra for fabricated pristine and NPs (CN) devices.

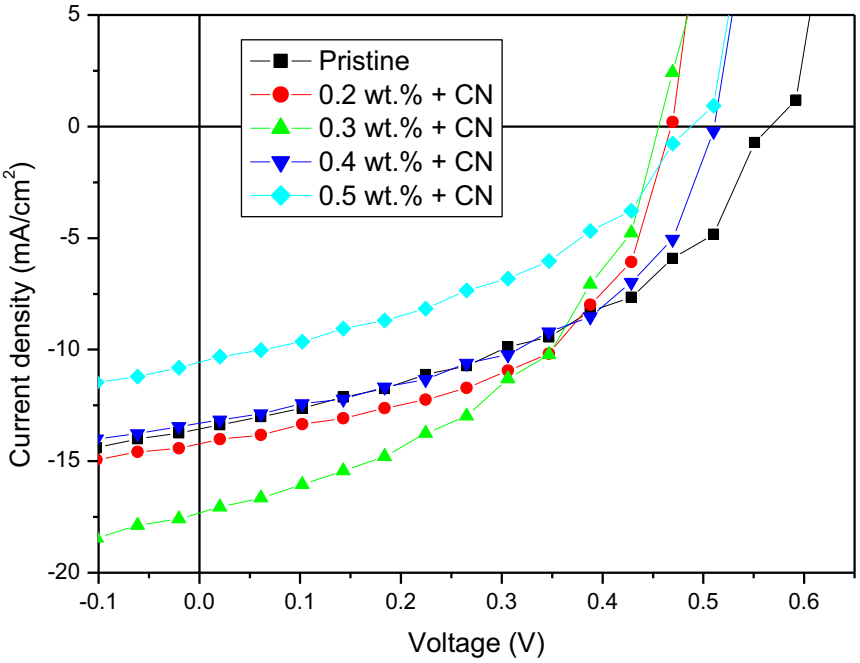

Figure 3: Current density – voltage curve for fabricated pristine and NPs (CN) devices

Table 1: Photovoltaic parameters for BHJ-OSCs with NPs and CN

	J_{sc} (mA/Cm^2)	V_{oc} (V)	FF	PCE (%)
Pristine	13.37	0.57	42.60	3.25
0.2 wt.% + CN	14.01	0.47	53.18	3.54
0.3 wt.% + CN	17.05	0.46	45.03	3.55
0.4 wt.% + CN	13.15	0.51	48.80	3.32
0.5 wt.% + CN	10.31	0.49	41.13	2.11

Carrier transport characteristics of the BHJ-OSCs designed with Cd doped $Ba(NO_3)_2$ nanoparticles and 1-chloronapthalene were investigated to examine the carrier mobility properties in the photoactive medium using the space charge limited current (SCLC) technique. The results on carrier mobility after the introduction of solvent additive (1-chloronapthalene) and Cd doped Ba $(NO_3)_2$ nanocomposites are summarized in Table 2. An increase in carrier mobility is observed as the NP concentration is reaches peak at 0.3 wt.%. Also, this increase in carrier mobility results in improved photocurrent generated and

PCE. Despite high carrier mobility attained, significant fraction of the carriers recombines before extraction at the electrodes owing in part to the low PCE obtained at 0.5 wt.% NPs.

Similarly, Oseni & Mola (2019) observed an increment of one order of magnitude in carrier mobility after introducing chloronapthalene in the photoactive layer which was higher than what was attained for the pristine device. Although, a higher carrier mobility was attained, it did not translate to a better photocurrent generated. In the same vein, Xie *et al.* (2013) revealed that introducing DIO solvent additive and trimetallic NPs in the absorber layer, carrier mobility jumped due to increase in exciton generation and separation. Increment in mobility was ascribed to the combination of light scattering of NPs and improved morphology of the absorber film by DIO additive. Furthermore, Oseni & Mola (2019) report that introducing solvent additive enhanced the crystallinity of the active layer improving carrier separation and mobility as clearly shown by the resulting mobility value (Table 2) and Jsc (Table 1). consequently, mobility of carriers intensely impacts the fill factor (Kaya *et al.,* 2012).

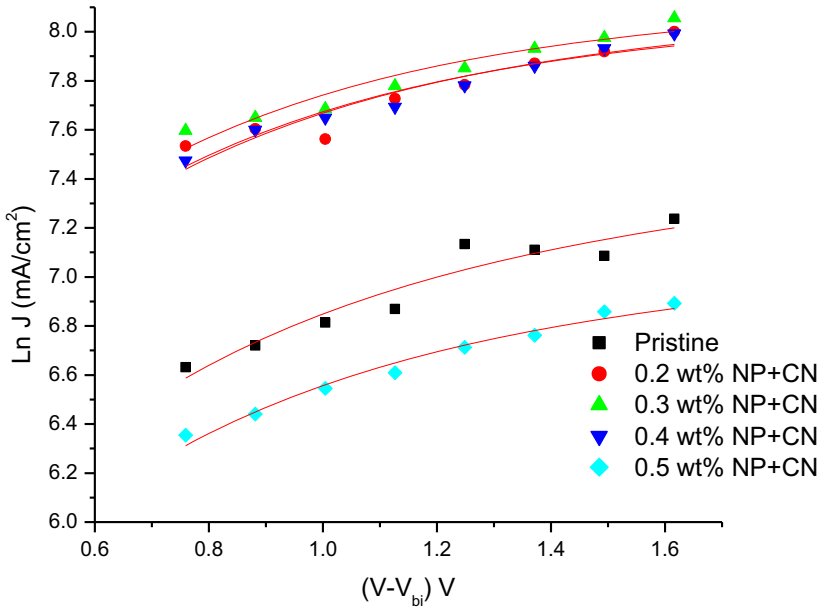

Figure 4: SCLC for pristine and NPs (CN) BHJ-OSCs

Table 2: Charge transport parameters of NP(CN) devices

	$\mu_o \times 10^{-2}$ ($cm^2V^{-1}s^{-1}$)	$\gamma \times 10^{-4}$ (cmV^{-1})
Pristine	1.55	-8.7
0.2 wt.% + CN	4.80	-9.9
0.3 wt.% + CN	5.32	-10.1
0.4 wt.% + CN	4.56	-9.8
0.5 wt.% + CN	1.32	-9.3

3.1 Structural analysis of the NPs

Transmission electron microscope (TEM) permits for the through imaging of nanoparticles, offering evidence on the size, and morphology of the nanoparticles as shown in Figure 5. Figure 5 shows the low magnification image of the Cd doped $Ba(NO_3)_2$ nanoparticles. Figures 5 and 6 show the high-resolution transmission electron microscope (HRTEM) image of nanoparticle which helps in studying the structure of individual NP. Figure 6b shows the elemental distribution of the Cd doped $Ba(NO_3)_2$ nanoparticles. Three elemental bonds can be seen i.e., Cd-O, Ba-O, and Ba-N. These elemental bonds play major role in the absorbance spectra in Figure 2. Also, the surface mapping of the NP indicating the crystallographic changes is shown in Figure 8, using the atomic force microscope (AFM). The XRD pattern of the NP is shown in Figure 9. Sharp diffraction peaks in the XRD corroborates that the NPs are crystalline.

The synthesized Cd doped Ba $(NO_3)_2$ nanocomposites are observed to have a spherical shape. The intermediate size of nanoparticles observed between 20 and 40 nm in diameter are used to usefully scatter the incident photon which improves the optical path, therefore enhancing the optical absorbance viewed in Figures 2. The little size of the NPs (5 - 20 nm in diameter) embedded in the absorber medium is attributed to cause near field effect or LSPR upon photoexcitation which causes an improvement of optical absorption (Lim *et al.,* 2016). In the same vein, metallic NPs (MNP) with average diameter 11 ± 0.2 nm were obtained for Au NPs and used in enhancing the PCE of fabricated devices (Otieno *et al.,* 2017). A cubic phase with hexagonal intense spots is observed from the SAED micrograph. It is noted that the interplanar distance estimated is around 0.27 nm for the structure. Also, the surface mapping of the nanoparticle shows the crystallographic changes using the AFM image which can be related to the XRD analysis. Similarly, the SAED pattern for Fe_4O_4 NPs studied by Kovalenko *et al.* (2019) showed the crystalline nature of the NPs due to the observed visible bright spots and seen in this current study.

It is established that the unit cell of the nanocomposite is of cubic perovskite structure from the XRD data with indexed peaks (100), (001), (200), (101), (110), (102), (012), (412), (411), (221), (113), (213), (613) and (308). Furthermore, it is proposed that various planes with highly pure phases are generated due to the peaks at different intensities. The estimated lattice constants, $a = 5.314$ Å *and* $b = 8.904$ Å, are in respectable understanding with the values recorded in the literature (JCPDS Card No. 31-174). The intense peaks indicate that the synthesised nanocomposites are crystalline. The calculated grain size of the nanocomposites was evaluated to be nearly 40 nm from the XRD analysis using the Debye-Scherrer formula.

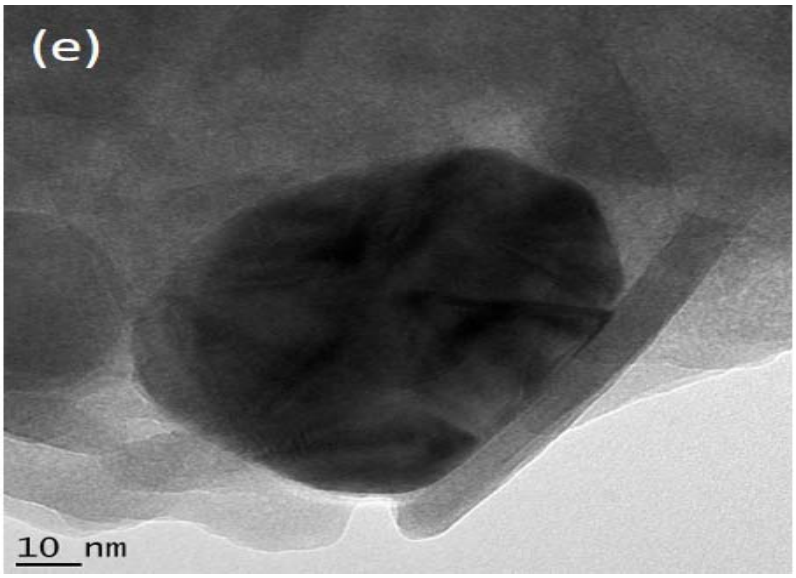

Figure 5: TEM image of Cd doped ($Ba(NO_3)_2$ NP

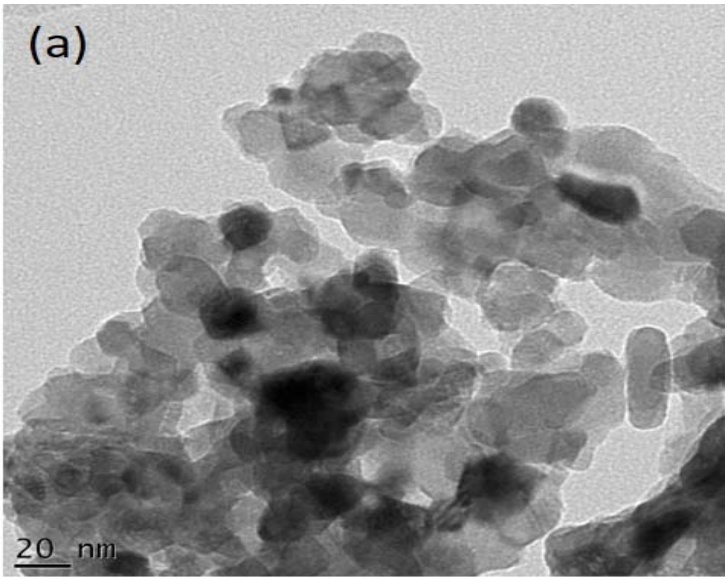

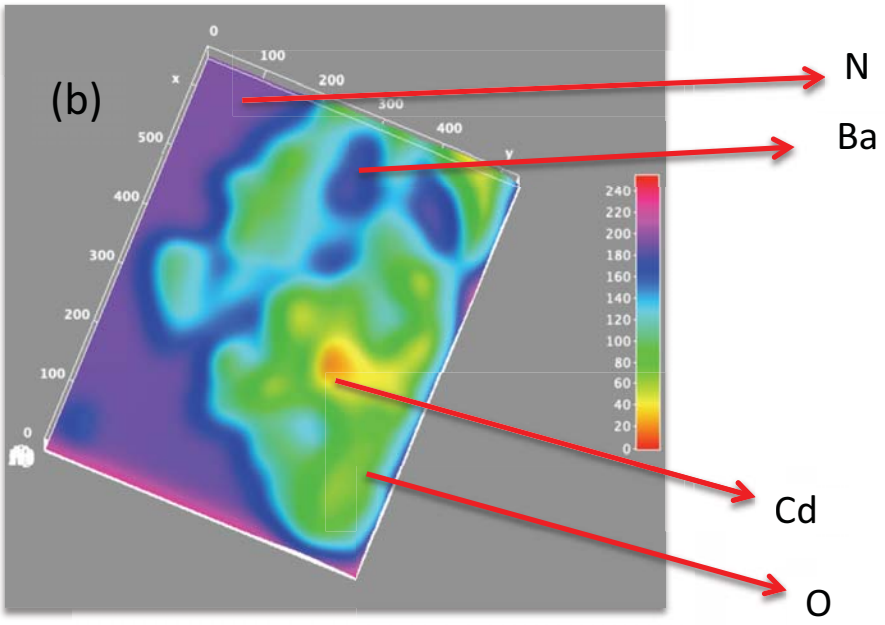

Figure 6: (a) HRTEM image of Cd doped ($Ba(NO_3)_2$ NP (b) elemental distribution of Cd doped ($Ba(NO_3)_2$ NP

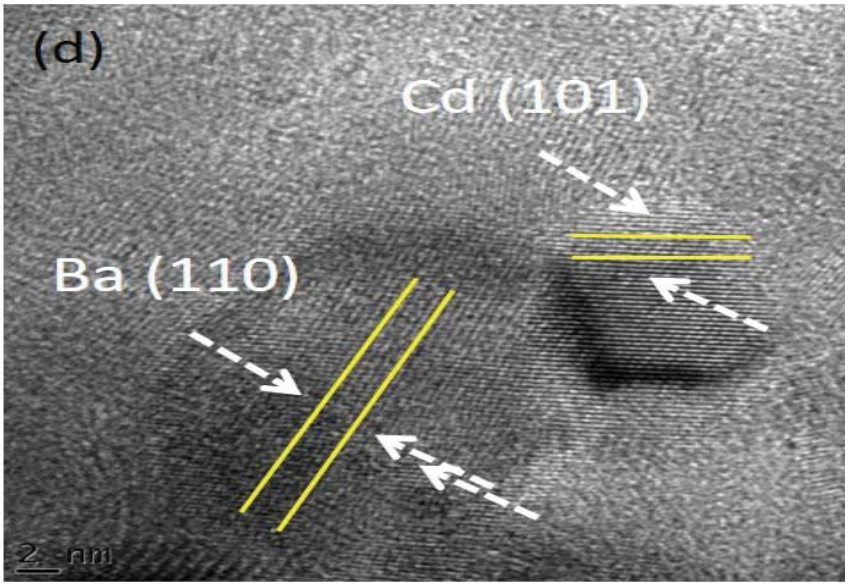

Figure 7: HRTEM image of Cd doped ($Ba(NO_3)_2$ NP

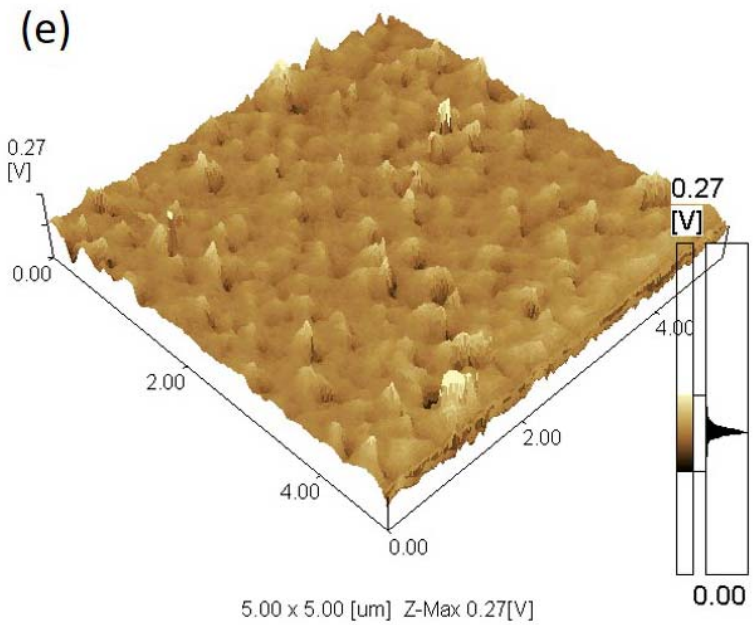

Figure 8: AFM of Cd doped ($Ba(NO_3)_2$ NP.

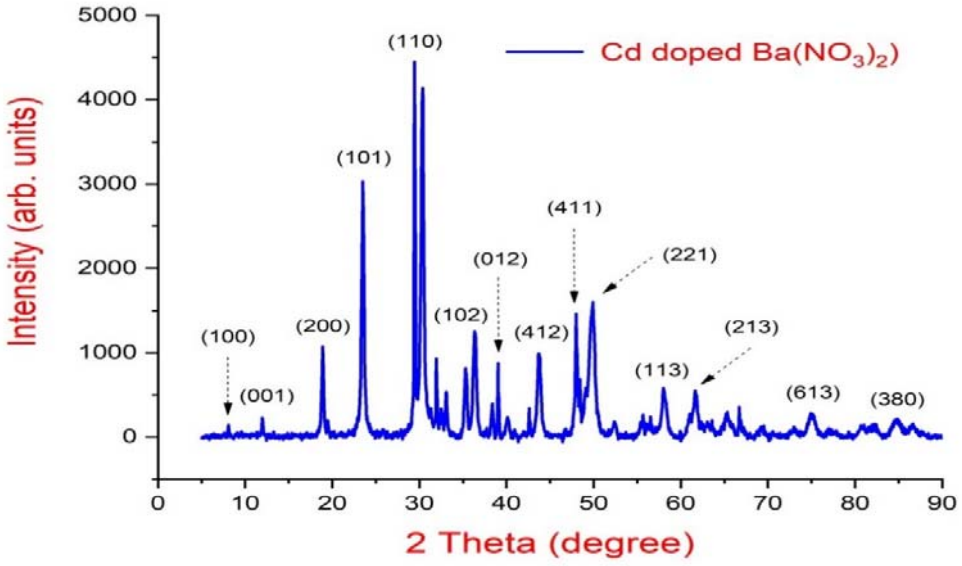

Figure 9: XRD graph of Cd doped Ba ($NO_3)_2$ NP (Kesinro *et al.,* 2019).

4. Conclusion

The effect of solvent additive on Cd:Ba ($NO_3)_2$ nanoparticles doped P3HT: PCBM based OSC was studied. Difference in device performances was noticed due to the various weight concentration of nanoparticles and solvent additive introduced during the preparation of the photoactive medium.

Consequently, significant enhancements were obtained from the devices fabricated with 0.3 wt.% NP and solvent additive resulting in an enhanced power conversion efficiency approximately 9.2 % in comparison to the pristine device. Also, the introduced solvent additive was observed to have improved the fill factor probably due to reduction of grain size of the polymer and fullerene domain resulting in reduced series resistance of the device. Also, it is assumed that due to the presence of elevated nongeminate recombination processes, the performances of the fabricated devices was not as high as expected after the introduction of nanoparticles and solvent additive Therefore, it can be concluded that to advance the performance of OSCs emphasis should be placed on the type of solvent additives and nanoparticles to be utilized. Also, the introduction of nanoparticles in different layers of the solar cell can be looked upon.

Acknowledgement
The authors are thankful to Covenant University for the funding offered for the publication of this article.

References

[1] Afolalu, S. A., Soetan, S. B., Ongbali, S. O., Abioye,A. A., & Oni, A. S. (2019). Morphological characterization and physio-chemical properties of nanoparticle – review, *IOP Conference Series: Materials Science and Engineering,* **640:** 012065, doi:10.1088/1757-899X/640/1/012065

[2] Berger, P. R. & Kim, M. (2018). Polymer solar cells: P3HT: PCBM and beyond, *Journal of Renewable and Sustainable Energy***, 10**: 013508. doi: 10.1063/1.5012992

[3] Ahmadi, M. H., Ghazvihi, M., Sadeghzadeh, M., Nazari, M. A., Kumar, R., Naeimi, A., & Ming, T. (2018). Solar power technology for electricity generation: A critical review. *Energy Science and Engineering,* **6:** 340 – 361.

[4] Huang J., Wang H., Yan K., Zhang X., Chen H., Li C.Z., & Yu J. (2017). Highly Efficient Organic Solar Cells Consisting of Double Bulk Heterojunction Layers. *Advanced Mater*ial, **29:**1606729.

[5] Kong T., Wang H., Liu X., Yu J., & Wang C. (2017). Improving the efficiency of bulk heterojunction polymer solar cells via binary-solvent treatment. *IEEE Journal of Photovoltaics,* **7:**214.

[6] Xing S., Wang H., Kong T., Yu J., Jiang J., & Wang C. (2017). Realization of performance enhancement in ternary polymer solar cells by broad absorption, efficient energy transfer, and balanced charge carrier mobility. *IEEE Journal of Photovoltaics*, **7:**1058.

[7] Vyprachticky, D., Demirtas, I., Dzhabarov, V., & Cimrova, V. (2017). New copolymers with thieno[3,2-b] thiophene or dithieno[3,2-b:2′,3′-d] thiophene units possessing electron withdrawing 4-cyanophenyl groups: synthesis and photophysical, electrochemical, and electroluminescent properties. *Journal of Polymer Science Part A: Polymer Chemistry,* 55**(16):** 2629–2638.

[8] Chen, W. & Zhang, Q. (2017). Recent progress in non-fullerene small molecule acceptors in organic solar cells (OSCs). *Journal of Materials Chemistry C*, **5:** 1275–1302.

[9] Seo, J. H., Gutacker, A., Sun, Y., Wu, H., Huang, F., Cao, Y., Scherf, U., Heeger, A. J., & Bazan, G. C. (2011). Improved high-efficiency organic solar cells via incorporation of a conjugated polyelectrolyte interlayer. *Journal of American Chemistry Society,* **133:** 8416–8419.

[10] Kaviyarasu, K., Mola, G. T., Oseni, S. O., Kanimozhi, K., Magdalane, C. M., Kennedy, J., & Maaza, M. (2019). ZnO doped single wall carbon nanotube as an active medium for gas sensor and solar absorber, *Journal of Materials Science: Materials in Electronics*, **30:**147–158.

[11] Choy, W. C. H. & Ren, X. (2016). Plasmon-electrical effects on organic solar cells by incorporation of metal nanostructures. *IEEE J. Sel. Top. Quantum Electron*, *22,* 4100209,

[12] Li, Z. B., Guan, X. X., Hua, Y. Q., & Hui, S. M. (2018). Composite nanostructures induced by water-confined femtosecond laser pulses irradiation on GaAs/Cresolar cell surface for anti-reflection. *Optic Laser Technology,* **106:** 222–227.

[13] Araújo, F. L., Amorim, D. R. B., Torres, B. B. M., Coutinho, D. J., & Faria, R. M. (2019). Effects of additive-solvents on the mobility and recombination of a solar cell based on PTB7-Th: $PC_{71}BM$. *Solar Energy* **177:** 284–292

[14] Oseni, S. O. & Mola, G. T (2019). Effects of metal-decorated nanocomposite on inverted thin-film organic solar cell, Journal of Physics and Chemistry of Solids 130 (2019) 120-126.

[15] Arbab, E. A. A. & Mola, G.T. (2019). Metals decorated nanocomposite assisted charge transport in polymer solar cell, *Materials Science in Semiconductor Processing*, **91:** 1-8.

[16] Tran, H. N., Kim, D. H., Park, S., & Cho, S. (2018). The effect of various solvent additives on the power conversion efficiency of polymer-polymer solar cells. *Current Applied Physics,* doi:10.1016/j.cap.2018.03.003.

[17] Jackson, N. E., Savoie, B. M., Marks, T. J., Chen, L. X., & Ratner, M. A. (2015). The Next Breakthrough for Organic Photovoltaics? *Journal of Physical Chemistry Letters,* **6:** 77-84.

[18] Liu, J et al., (2001). Solvation-induced morphology effects on the performance of polymer-based photovoltaic devices, *Advanced Functional Material,* **11:** 420–424.

[19] Oseni, O. S. & Mola, G. T. (2019). Effects of metal-decorated nanocomposite on inverted thin film organic solar cell, *Journal of Physics and Chemistry of Solids,* **130:** 120–126.

[20] Foertig, A., Kniepert, J., Gluecker, M., Brenner, T., Dyakonov, V., Neher, D., & Deibel, C. (2014). Nongeminate and geminate recombination in PTB7: PCBM solar cells. *Advanced Functional Material,* **24:**1306.

[21] Otieno, F., Shumbula, N. P., Airo, M., Mbuso, M., Moloto, N., Erasmus, R. M., … Wamwangi, D. (2017). Improved efficiency of organic solar cells using Au NPs incorporated into PEDOT: PSS buffer layer. *AIP Advances, 7*(8), 085302.

[22] Tong, T. M., Asare, J., Rwenyagila, E. R., Anye, V., Oyewole, O. K., Fashina, A. A., & Soboyejo, W. O. (2015). A study of factors that influence the adoption of solar powered lanterns in a rural village in Kenya, *Perspectives on Global Development and Technology*, 14**(4):** 448–491.

[23] Xie, F.-X., Choy, W. C. H., Sha, W. E. I., Zhang, D., Zhang, S., Li, X., Leung, X. & Hou, J. (2013). Enhanced charge extraction in organic solar cells through electron accumulation effects induced by metal nanoparticles. *Energy Environment and Science, 6,* 3372–3379.

[24] Ono L.K., Leyden M.R., Wang S., & Qi Y. (2016). Organometal halide perovskite thin films and solar cells by vapor deposition. *Journal of Material Chemistry A*, **4:** 6693.

[25] Wang Y., Li S., Zhang P., Liu D., Gu X., Sarvari H., Ye Z., Wu J., Wang Z., & Chen Z.D. (2016). Solvent annealing of PbI_2 for the high-quality crystallization of perovskite films for solar cells with efficiencies exceeding 18%, *Nanoscale*, **8**:19654

[26] Dlamini, M.W., & Mola, G. T. (2019). Near-field enhanced performance of organic photovoltaic cells, *Physica B: Condensed Matter,* 552: 78-83.

[27] Kesinro, O. R., Boyo, A. O., Hamed, M.S.G., Akinyemi, M. L., Maaza, M., Kasinathan. K. & Mola, G. T. (2019). Cd doped $Ba(NO_3)_2$ nanoparticle asbroadband solar absorber in thin film organic solar cell, *Polymers Composites,* 1-7.

[28] Abodunrin, T. J., Boyo, A. O., Usikalu, M. R. & Kesinro, O. (2018). Spectral responses of *B.vulgaris* dye-sensitized solar cells to change in electrolyte, *IOP Conf. Series: Earth and Environmental Science,* **173:** 012047.

[29] Ergete, A., Fedlu K. Sabir, F. K., Li, Y., & Yohannesa, T. (2015). Effect of solvent additives and P3HT on PDTSTT/PCBM-based bulk heterojunction solar cells. *Journal of Photonics for Energy, 5,* 057209-057210.

[30] Fleetham, T., Choi, J.-Y., Choi, H. W., Alford, T., Jeong, D. S., Lee, T. S.,Lee, W. S., Li, J. & Kim, I. (2015). Photocurrent enhancements of organic solar cells by altering dewetting of plasmonic Ag nanoparticles. *Scientific Report, 5*(1), 14250.

[31] Green, M. A., Emery, K., Hishikawa, Y., Warta, W., Dunlop, E. D., Levi, D. H., & Ho-Baillie, A. W. Y. (2016). Solar cell efficiency tables (version 49*). Progress in Photovoltaics: Research and Applications, 25*(1), 3–13. doi:10.1002/pip.2855.

[32] Lim, E. L., Yap, C. C., Mat Teridi, M. A., Teh, C. H., Mohd Yusoff, A. R., & Hj Jumali, M. H. (2016). A review of recent plasmonic nanoparticles incorporated P3HT: PCBM organic thin film solar cells. *Organic Electronics, 36,* 12–28.

[33] Liu, J et al., (2001). Solvation-induced morphology effects on the performance of polymer-based photovoltaic devices. *Advanced Functional Material, 11,* 420–424.

[34] Kaya, E., Apaydin, D. H., Yildiz, D. E., Toppare, L., & Cirpan, A. (2012). Solution processable benzotriazole and fluorene containing copolymers for photovoltaic applications. *Solar Energy Materials and Solar Cells, 99,* 321–326.

[35] Kovalenko, A., Yadav, R. S., Pospisil, J., Zmeskal, O., Karashanova, D, Heinrichová, P.,… Weiter, M. (2016). Towards improved efficiency of bulk heterojunction solar cells using various spinel ferrite magnetic nanoparticles, *Organic Electronics*, *39,* 118-126.

[36] Perez, M. D., Borek, C., Forrest, S. R., & Thompson, M. E. (2009). Molecular and morphological influences on the open circuit voltages of organic photovoltaic devices. *Journal of American Chemistry Society, 131,* 9281–9286.

[37] Song, X., Gasparini, N., & Baran, D. (2017). The influence of solvent additive on polymer solar cells employing fullerene and non-fullerene acceptors. *Advanced Electronic Material,* 1700358.

[38] Choi, H., Ko, S.-J., Kim, T., Morin, P.-O., Walker, B., Lee, B. H., Leclerc, M., Kim, J. Y., & Heeger, A. J. (2015). Small-bandgap polymer solar cells with unprecedented short-circuit current density and high fill factor. *Advanced Material, 27,* 3318 – 3324.